nature climate change

SUPPLEMENTARY INFORMATION

DOI: 10.1038/NCLIMATE3108

Remotely sensed resilience of tropical forests

Jan Verbesselt[1], Nikolaus Umlauf[2], Marina Hirota[3,4], Milena Holmgren[5] , Egbert H. Van Nes[5], Martin Herold[1], Achim Zeileis[2] and Marten Scheffer[4]

November 16, 2015

[1] Laboratory of Geo-Information Science and Remote Sensing, Wageningen University, 6708 PB, Wageningen, The Netherlands
[2] Department of Statistics, Faculty of Economics and Statistics, Universität Innsbruck, Universitätsstr. 15, 6020 Innsbruck, Austria
[3] Department of Physics, Federal University of Santa Catarina, 88040–900, Florianopolis, Brazil.
[4] Environmental Sciences Department, Wageningen University, P.O. Box 47, 6700 AA, Wageningen, The Netherlands
[5] Resource Ecology Group, Wageningen University, P.O. Box 47 , 6700 AA, Wageningen, The Netherlands

1 Data sets and sampling strategy

1.1 Optical and microwave satellite data

Optical MODIS Normalized Difference Vegetation Index (NDVI) is derived from the bidirectional reflectance distribution function (BRDF) adjusted reflectance measurements (MCD43C4 version 5, 2000–2011, 5.6km). The reflectance product MCD43C4 provides reflectance data adjusted using a BRDF to model the values as if they were taken from nadir view to account for potential artefacts introduced by varying sun-sensor geometry[1]. Both Terra and Aqua MODIS sensor data are used in the generation of this product, providing the highest probability for quality input data and designating it as an MCD, meaning Combined, product. Fill values and measurements with a low BRDF inversion quality (50% of more fill values) are excluded from the analysis. The effect of excluding measurements with low BRDF inversion quality (e.g., 50% of more fill values) on the results has been studied (results not shown) and did not influence the effect of MAP and TAC (see Section 4). The 8-day BRDF corrected NDVI values are aggregated to monthly mean NDVI values to facilitate comparison with other data sets and reduce noise due to BRDF and cloud effects[2,3].

The MODIS NDVI data, despite the corrections and temporal compositing, still contains residual invalid measurements (e.g., cloud effects). The quality flags are used to remove all invalid observations and also derive the percentage of invalid measurements per pixel through the whole time span as a summary of cloud and atmospheric effects. We include the maximum number of consecutive and percentage of invalid measurements in our modeling approach to

 DOI: 10.1038/NCLIMATE3108

account for the influence of clouds and atmospheric effects (Section 3).

Vegetation Optical Depth data (VOD) from the Advanced Microwave Scanning Radiometer - Earth Observing System (AMSR-E, July 2002–2011, 0.25 degree spatial resolution) are used [4]. VOD represents water content in aboveground woody and leaf biomass and is sensitive to long-term climate changes. Unlike NDVI, the microwave VOD are least affected by atmospheric and weather conditions[4,5]. Also, satellite microwave observations have shown that forest in western Amazonia experienced a strong water deficit during the dry season of 2005 and the slow recovery (> 4 year) of forest canopy structure[6]. The presence of open water affects the microwave emissions and may lead to underestimates of VOD values [7]. Because of this, regions with extensive lakes, reservoirs, rivers and flooded vegetation were masked out [4,8].

In summary, the NDVI, operating in the optical regime, is sensitive to chlorophyll abundance and photosynthetically active biomass of the leaves, whereas the microwave-based VOD is an indicator of the vegetation water content in total above ground biomass, i.e., including wood and leaf components[4]. Previous studies indicate that the fluctuations in VOD typically correlated to precipitation variations, and that the mutually independent VOD and NDVI do not necessarily respond in identical manners[9]. Considering both products together provides a more robust assessment of long-term vegetation dynamics at the global scale.

1.2 Precipitation and temperature data

Mean annual precipitation (`MAP`) and mean annual temperature (`MAT`) from 1962–2011 is derived from the *Climatic Research Unit* (CRU) monthly rainfall and minimum temperature data set (http://badc.nerc.ac.uk/browse/badc/cru). Decelerating growth rates in tropical forest trees have been reported to be linked with increasing annual mean daily minimum temperatures and decreasing mean annual precipitation[10,11]. The latest and currently longest global precipitation product is used, i.e., CRU TS 3.20[12] (0.5° by 0.5°).

We also used precipitation data from the Tropical Rainfall Measuring Mission (TRMM; 3B42-v6; monthly, 0.25°) for the period of 1998–2011 to derive `MAP` at a higher spatial resolution when compared to the CRU data set. The satellite observations of rainfall from TRMM has been able to capture patterns of rainfall magnitude and seasonality undetected by CRU due to lack of operating ground stations, particularly over the past decade[13,14] (Figure S1).

DOI: 10.1038/NCLIMATE3108

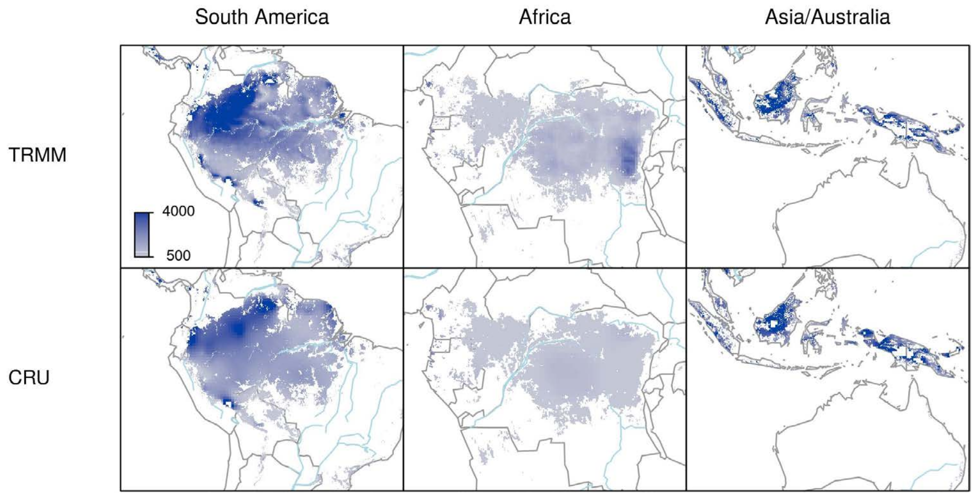

Figure S1: Mean Annual Precipitation (`MAP`, mm/year) derived from monthly TRMM (2000–2011) and CRU (1962–2011) data sets.

1.3 Soil fertility data

In addition, as a potential explanation of spatial patterns of slowing down of vegetation activity in the pan-tropics, the Total Exchangeable Bases (TEB) of the top soil, as provided by the harmonised world soil database[15], is included in the model (see Figure S3 and Section 3).

1.4 Sampling strategy for selecting intact and undisturbed evergreen tropical forests

The centroid of each MODIS raster cell is used to sample NDVI time series, percentage tree cover and `MAP`, soil TEB for the intact and undisturbed evergreen forests in the tropics (35° S and 15° N). The sampled data is then used to assess the continent specific relationship between NDVI based measures of critical slowing down and environmental variables (e.g., `MAP`). Figure S1 illustrates the mean annual precipitation derived from monthly TRMM (2000–2011) and CRU (1962–2011) data in the pan-tropics.

We concentrated the analysis on forested areas with tree cover higher than 60%[16] based on the MODIS percentage tree cover product and selected intact and undisturbed evergreen tropical forests of Africa, South America and South East Asia. We selected intact forest using the intact forests reported by the World Intact Forest Landscape (IFL) map (`http://www.intactforests.org/`,[17]).

DOI: 10.1038/NCLIMATE3108

We selected only evergreen tropical forest and excluded the human impacted, bare or flooded areas reported by the Global Land Cover 2000 product (GLC2000,[18]). The percentage tree cover for the year 2010 is derived from MODIS vegetation continuous fields product (MOD44B, version 5, spatial resolution 250m). The world's IFL map is a spatial database (scale 1:1,000,000) that shows the extent of the intact forest landscapes (IFL) for year 2000. Intact forests are selected when more than 90% of the MODIS pixels are intact as indicated by the IFL raster layer. Undisturbed evergreen forests are identified using the GLC2000 when less than 10% of the pixels had experienced intensive human impacts (codes: 16–18, and 22) or were bare or flooded (codes: 15 and 19–21)[19].

2 Indicators of slowing down

We employ the temporal autocorrelation (`TAC`) of the NDVI time series as the main indicator of slowing down. As `TAC` varies substantially over space and time, the `TAC` is determined individually for each pixel so that the resulting estimates cannot be confounded with spatial correlations. Moreover, we account for the possibility that the `TAC` itself varies over time while adjusting long-term trends and seasonal periodic patterns. Specifically, each pixel is first detrended (including seasonal adjustment) and subsequently the `TAC` of the detrended NDVI is computed using two different methods.

2.1 Detrending

In order to obtain an accurate estimate of `TAC`, time series need to be stationary without long-term trends or seasonal periodic patterns[20,21] (just called "trends" in the following). Otherwise, if trends are not accounted for, the `TAC` estimate may be biased. Fortunately, deterministic trends can be removed efficiently without the need for specifying the `TAC` pattern (see Fuller, 1996, pp. 476–480)[22].

To select a detrending method that is most appropriate for time series with potentially time-varying seasonal amplitude (i.e., size of the seasonal effect) and phase (i.e., start of the season) we conducted an extensive simulation study (paper in preparation). In the simulation study, we assessed how well various methods from the literature can detrend artificial time series with typical characteristics of NDVI and VOD time series data[23,24]. More precisely, we considered artificial time series with all combinations of several long-term trend patterns (none, linear, smoothly varying), seasonal patterns (none, cyclical, time-varying amplitude and phase), and `TAC` patterns (none, constant, linear, smoothly varying). The considered detrending methods are: linear filtering (Holt-Winters with additive or multiplicative season)[25,26], Kalman filtering using state space models (with potentially time-varying trend and seasonal pattern)[27], linear regression (linear trend with harmonic seasonal pattern), additive regression (smooth long-term trend with either smooth cyclical or time-varying seasonal pattern)[28–30], and LOESS smoothing (with smooth long-term trend and either stable or smoothly varying seasonal pattern)[31].

The result of the simulation study illustrates that many of the various detrending methods lead to qualitatively similar results and can reliably recover both the trend and the TAC. However, not surprisingly, if amplitude/phase are indeed time-varying in the simulation, methods that allow for such flexibility perform clearly better. To make sure that our results are robust against many conceivable trend patterns, we employ three particularly well-performing models in the following: season-trend decomposition by LOESS smoothing (STL)[31], decomposition based on additive models including time-varying harmonic seasonal effects (STA)[30] and extended Kalman filtering of state space model (SSM)[27] with time-varying parameters to capture smoothly varying and dynamically changing trends, respectively. An advantage of the STA and SSM when compared to the STL approach is that no interpolation of missing data is required. Furthermore, to ensure stationarity of the detrended series KPSS tests[32] are carried out.

Figure S2 illustrates the ability of the detrending methods used to model highly complex time trends and seasonal patterns. Figure S2 illustrates that all, slowly and smoothy vary periodic patterns have been removed prior to computing TAC. What the Figure S2 shows is that here dryer regions tend to have higher TAC (i.e. slower recovery times after disturbance). The key point here is that the TAC has been estimated from time series from which all potential deterministic patterns, i.e. long-term trends and time-varying seasonality have been removed. All potentially occurring trend and seasonal variation has been removed using an “ensemble” of detrending methods to enable a “true” TAC estimate[21,33].

DOI: 10.1038/NCLIMATE3108

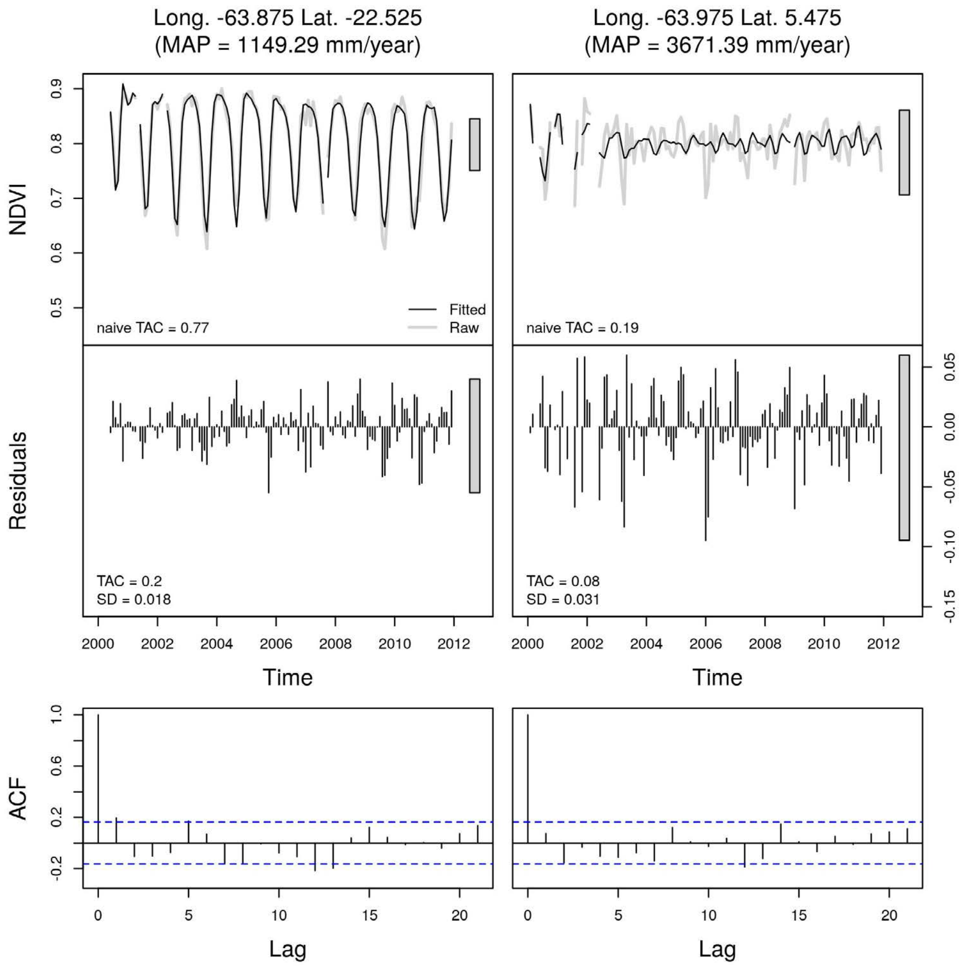

Figure S2: Examples of detrending of undisturbed forest NDVI time series using the STA in South America. The left column represents a time series of a pixel with low MAP and pronounced seasonality, the right column high MAP and less pronounced seasonality. The top row shows the raw NDVI time series in gray versus the fitted times series from the STA in black. Both cases suggest accurate detrending although both time series exhibit time-varying seasonal patterns and data gaps. The residuals indicate stationarity which is also confirmed by the KPSS test. The estimated ACF1 at higher lags also suggests no remaining significant seasonal patterns. The reported TAC estimates derived from the ACF1 method are higher for the drier forest pixel. The SD results are rather similar. The corresponding interquartile range of the estimated 2 year ACF1 rolling method is 0.15–0.31 (mean 0.18) for the low MAP pixel and 0.09–0.15 (mean 0.09) for high MAP pixel.

2.2 TAC estimation

After removing long-term trends and seasonal patterns individually for each pixel, TAC and SD can simply be estimated by the corresponding full-sample estimators. In case of TAC, we simply employ the empirical autocorrelation function at lag 1 (ACF1). Moreover, to account for possible time-varying effects in TAC that could affect TAC over the whole observation period, we applied a two year rolling window ACF1 approach[20].

Combining the three detrending methods (STL, STA and SSM) with the two TAC estimators above yields six possible combinations (see Table S1). In all subsequent analyzes we always report results of this ensemble of six method combinations in order to demonstrate that all conclusions are robust against the methods for detrending and TAC estimation.

Detrend method	TAC method
STL	ACF1
STL	ACF1 roll
STA	ACF1
STA	ACF1 roll
SSM	ACF1
SSM	ACF1 roll

Table S1: Overview of all combinations of the detrending and TAC methods.

3 Models

To avoid potential bias in TAC and SD estimates (Section 2) when the time series contain a large number of missing values by the exclusion of bad quality measurements (Section 1.1), strict quality criteria are used to exclude time series with a percentage of missing values (further referred to as %NAs) larger than 10%, as well as time series containing more than 2 consecutive missing values, i.e., maximum of 2 months, further referred to as NA maxgap. To further reduce the influence by clouds and haze, locations with mean annual precipitation (MAP) of more than 4000 mm are excluded similar to Hirota et al.[16]. The total number of time series analysed for the different satellite data sets and detrending methods is shown in Table S2.

We assessed the relationship of TAC and SD of intact evergreen forest pixels with environmental covariates using additive regression models[28,34,35]. Since TAC and SD estimates may vary by the detrending and TAC methods used, we estimated an ensemble of the 6 different detrending and TAC method combinations (see Table S1) for each of the two data sets (see Table S2).

 DOI: 10.1038/NCLIMATE3108

Data set	Continent	# Obs. STL	# Obs. STA	# Obs. SSM
MODIS NDVI	South America	41492	40833	40806
	Africa	21701	21511	21501
	Asia/Australia	7630	7324	7318
VOD	South America	4897	4897	4897
	Africa	889	889	889
	Asia/Australia	374	374	374

Table S2: Number of time series observations (# Obs.) analysed for different continents, data sets (MODIS NDVI 2000–2011, VOD 2002–2011), and detrending methods (STL, STA and SSM).

The main explanatory variable of interest is `MAP` derived from TRMM data (see Section 1.2). To asses the influence of other environmental variables like percentage tree cover (`%Trees`), the effect of varying seasonality (`Season`, estimated as the amplitude of the seasonal component using STL decomposition[31]), `TAC` and `SD` of precipitation time series (`PreTAC`, `PreSD`, derived from the detrended precipitation time series), mean annual temperature (`MAT`), the soil fertility (`Soil`) or by `%NAs` (as a proxy for cloud cover), we estimated additive models given by

$$\begin{aligned}\texttt{TAC} \;=\; & \gamma_0 + f_1(\texttt{MAP}) + f_2(\texttt{\%Trees}) + f_3(\texttt{Season}) + f_4(\texttt{PreTAC}) + \\ & f_5(\texttt{MAT}) + f_6(\texttt{Soil}) + f_7(\texttt{\%NAs}) + f_8(\texttt{Long},\texttt{Lat}) + \varepsilon \quad \varepsilon \sim N(0,\sigma^2), \qquad (1)\end{aligned}$$

where for models with `SD` as the response variable `PreTAC` is exchanged by `PreSD`. Also note that the effect of `%NAs` is not included using VOD data, since the time series do not contain missing values. The parameter γ_0 is the usual model intercept, the functions $f_1,\ldots,f_7$ are smooth functions and are modeled by splines. Furthermore, function f_8 accounts for spatial effects of longitude and latitude pixel coordinates on `TAC` or `SD`, i.e., the function models spatial variation due to factors like dry season length, fire frequency, topography and potential herbivory effects, that have not been measured[19].

4 Results

When computing the KPSS test on a 5% significance level, all detrending methods generated stationary time-series. Table S3 shows the percentage rates of pixels that according to the KPSS test are stationary. 98% of all VOD and 93-98% of all MODIS time-series selected for analysis (see sampling strategy) are stationary.

DOI: 10.1038/NCLIMATE3108

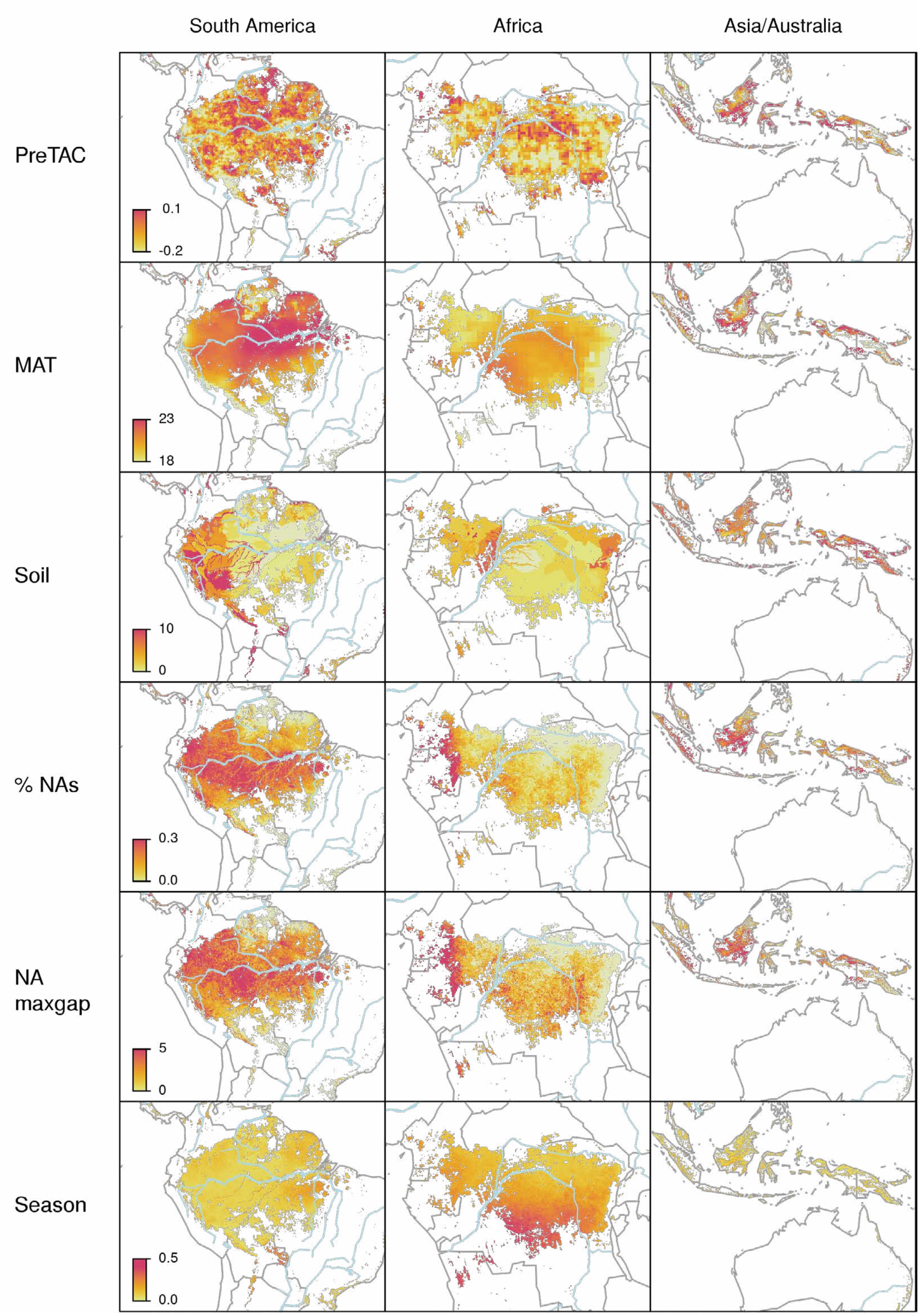

Figure S3: Continent-specific maps of detrended TRMM precipitation temporal autocorrelation (`PreTAC`), mean annual CRU temperature (`MAT`), soil fertility (`Soil`), percentage missing observations (`%NAs`), maximum number of consecutive missing observations (`NA maxgap`) in the MODIS NDVI time series and seasonal amplitude of the NDVI time series (`Season`).

 DOI: 10.1038/NCLIMATE3108

Detrend method	KPSS test
VOD SSM	0.989
VOD STL	0.990
VOD STA	0.986
MODIS SSM	0.932
MODIS STL	0.981
MODIS STA	0.935

Table S3: Percentage rates of pixels that according to the KPSS test are stationary at a 5% significance level. The percentages are calculated for selected MODIS and VOD based time series following the sampling strategy described above.

4.1 Environmental effects on TAC

Models are fitted per continent for all combinations of detrending and TAC methods (see Section 2, Table S1 and Section 3) to study the influence of MAP on TAC.

The MAP effect on TAC is similar across continents and satellite derived MODIS NDVI and VOD data sets (Figures S4 and S5). It is shown that for a decreasing MAP the TAC increases while accounting for a all other relevant environmental variables (%Trees, Soil, MAT), and potential data driven effects like seasonality (Season) and data quality (%NAs) of the NDVI signal and TAC derived from precipitation (PreTAC). The MAP and Season are the two most important variables and show that for decreasing MAP (i.e., increasing dryness) the TAC increases while seasonality increases (e.g., forest types showing more seasonality). This confirms that dryer evergreen forest are slowing down while showing more seasonal variability for decreasing tree cover percentages (%Trees).

Across different continents, the temporal autocorrelation of precipitation (PreTAC) has no effect on TAC. Furthermore, it is shown that TAC is increasing with increasing MAT (the only exception being the NDVI pattern for Africa, Figure S4). This could illustrate earlier reported findings that decelerating growth rates in tropical forest trees are linked with increasing mean annual temperature[10,11].

The estimated ensemble mean levels of TAC (the intercept γ_0 in Eq. 1) for all data sets and continents are shown in Table S4. According to MODIS and VOD data, the estimates suggest that the mean level of TAC is the lowest in Africa.

	Continent		
Data set	South America	Africa	Asia/Australia
MODIS NDVI	0.15 (0.00046)	0.08 (0.00057)	0.18 (0.00109)
VOD	0.19 (0.00151)	0.13 (0.00298)	0.14 (0.00512)

Table S4: Estimated ensemble mean (intercepts γ_0 in Eq. 1) and standard error of the derived `TAC` of all data sets, detrending and `TAC` methods.

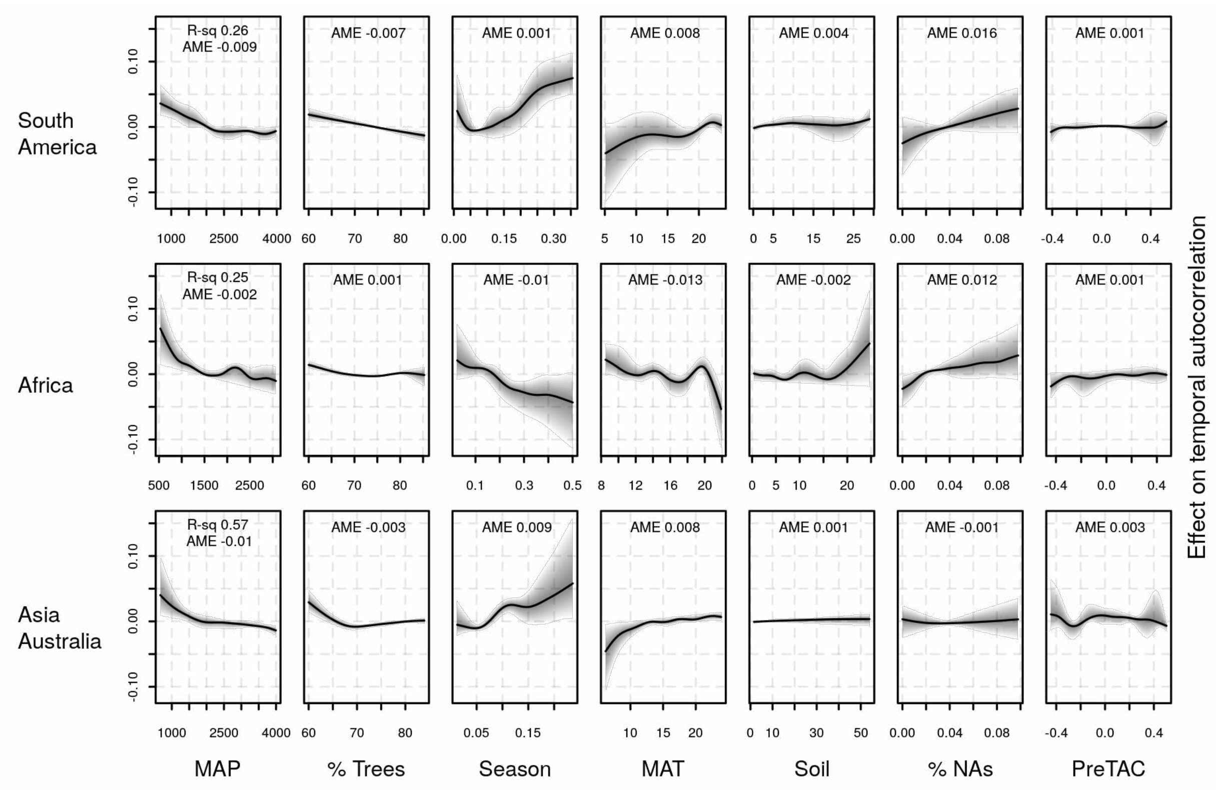

Figure S4: Estimated effects for all terms of model (Eq. 1) on `TAC` using NDVI MODIS (2000–2011), derived from different detrending and `TAC` methods. The black solid lines represent the mean curve from an ensemble of six curves (i.e., three detrending methods and two indicators of temporal autocorrelation). The gray shaded area highlights the range of the six individual ensemble members. The average R^2 and Average Marginal Effect (AME) are reported in the top range of the plots.

 DOI: 10.1038/NCLIMATE3108

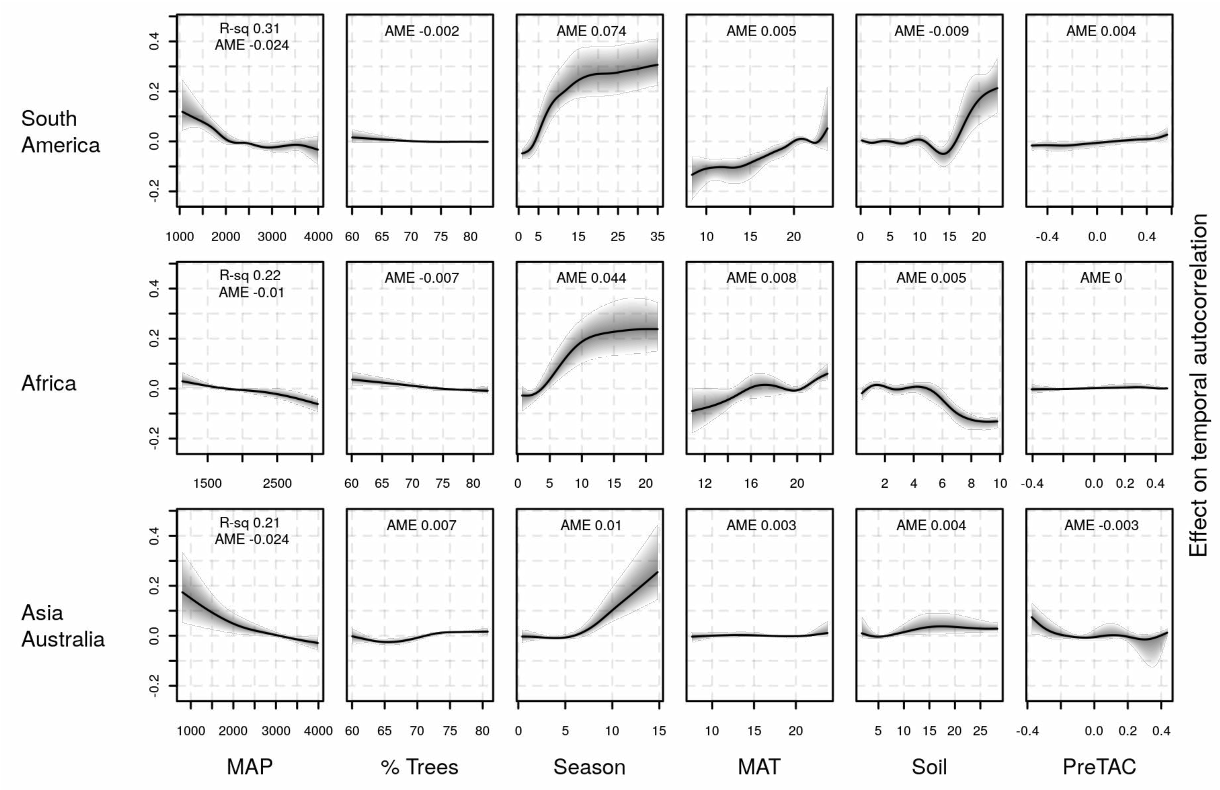

Figure S5: Estimated effects for all terms of model (Eq. 1) using the VOD (2002-2011), derived from different detrending and TAC methods. The black solid lines represent the mean curve from an ensemble of six curves (i.e., three detrending methods and two indicators of temporal autocorrelation). The gray shaded area highlights the range of the six individual ensemble members. The average R^2 and Average Marginal Effect (AME) are reported in the top range of the plots.

4.2 Environmental effects on SD

Figures S6 and S7 illustrate that the MAP and other environmental variables except the varying seasonality (Season), have a minor effect on SD variation as shown in the y-axis. The models explaining SD variability do not show clear patterns for the MAP effect as we obtain when modeling TAC.

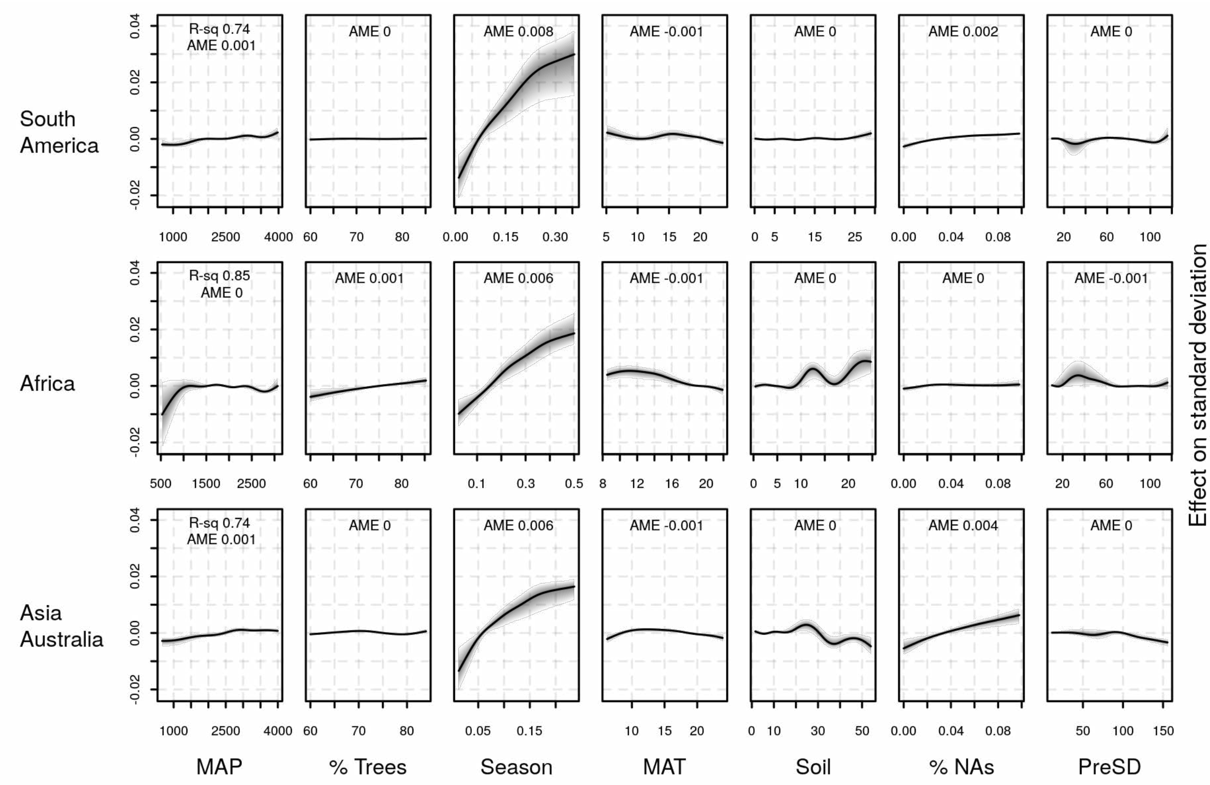

Figure S6: Estimated effects for all terms of model (1) on SD using NDVI MODIS (2000–2011), derived from different detrending methods. The black solid lines represent the mean curve from an ensemble of six curves (i.e., three detrending methods and two indicators of temporal auto-correlation). The gray shaded area highlights the range of the six individual ensemble members. The average R^2 and Average Marginal Effect (AME) are reported in the top range of the plots.

DOI: 10.1038/NCLIMATE3108

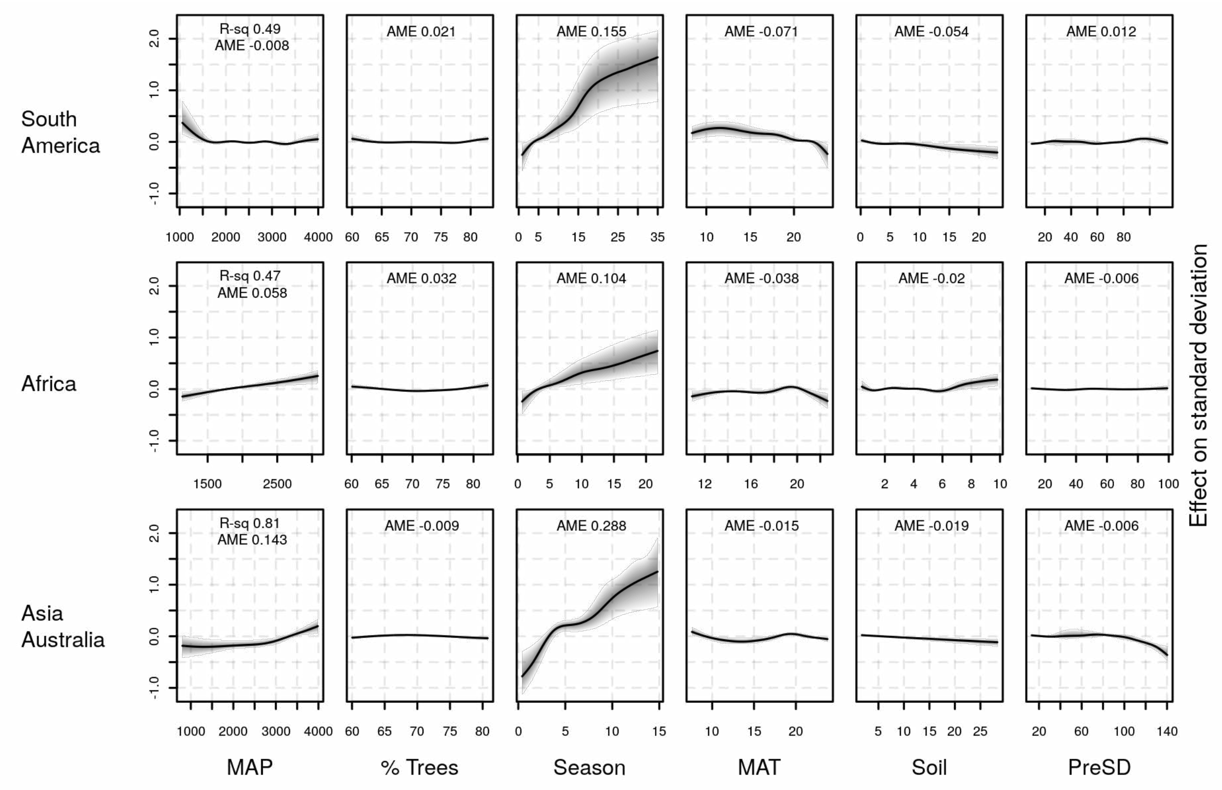

Figure S7: Estimated effects for all terms of model (1) using VOD (2002-2011), derived from different detrending methods. The black solid lines represent the mean curve from an ensemble of six curves (i.e., three detrending methods and two indicators of temporal autocorrelation). The gray shaded area highlights the range of the six individual ensemble members. The average R^2 and Average Marginal Effect (AME) are reported in the top range of the plots.

5 Software

The analysis is fully processed within the statistical environment R[36] version 3.1.0. For satellite image manipulation we used the **raster**[37] and **bfast**[23] package (`http://bfast.R-Forge.R-project.org/`). Detrending using the state-space model is based on the **sspir**[38,39] package, all models were fitted by the **mgcv**[40] package.

6 Acknowledgments

This research was partly funded by a Marie-Curie IRG grant within the European Community's Seventh Framework Program to J.V. (268423, http://bfast.r-forge.r-project.org/) and by the ERC-Early Warning grant and Spinoza award received by MS. We thank Yi Liu for the global VOD data set (2002-2011).

References

1. Morton, D. C. *et al.* Amazon forests maintain consistent canopy structure and greenness during the dry season. *Nature News* 1–16 (2014).

2. Frey, R. A. *et al.* Cloud detection with MODIS. part i: Improvements in the MODIS cloud mask for collection 5. *Journal of Atmospheric and Oceanic Technology* **25**, 1057–1072 (2008).

3. Poulter, B. & Cramer, W. Satellite remote sensing of tropical forest canopies and their seasonal dynamics. *International Journal Of Remote Sensing* **30**, 6575–6590 (2009).

4. Liu, Y. Y., van Dijk, A. I. J. M., McCabe, M. F., Evans, J. P. & de Jeu, R. A. M. Global vegetation biomass change (1988-2008) and attribution to environmental and human drivers. *Global Ecology and Biogeography* **22**, 692–705 (2013).

5. Asefi-Najafabady, S. & Saatchi, S. Response of African humid tropical forests to recent rainfall anomalies. *Philosophical Transactions of the Royal Society B-Biological Sciences* **368**, 20120306 (2013).

6. Saatchi, S. *et al.* Persistent effects of a severe drought on Amazonian forest canopy. *Proceedings of the National Academy of Sciences* **368**, 20120312–20120312 (2012).

7. Jones, M. O., Jones, L. A., Kimball, J. S. & McDonald, K. C. Satellite passive microwave remote sensing for monitoring global land surface phenology. *Remote Sensing Of Environment* **115**, 1102–1114 (2011).

8. Lehner, B. & Döll, P. Development and validation of a global database of lakes, reservoirs and wetlands. *Journal of Hydrology* **296**, 1–22 (2004).

9. Zhou, L. *et al.* Widespread decline of Congo rainforest greenness in the past decade. *Nature News* 1–18 (2014).

10. Feeley, K. J., Joseph Wright, S., Nur Supardi, M. N., Kassim, A. R. & Davies, S. J. Decelerating Growth in Tropical Forest Trees. *Ecology Letters* **10**, 461–469 (2007).

11. Galbraith, D. *et al.* Multiple mechanisms of amazonian forest biomass losses in three dynamic global vegetation models under climate change. *New Phytologist* **187**, 647–665 (2010).

12. Mitchell, T. D. & Jones, P. D. An improved method of constructing a database of monthly climate observations and associated high-resolution grids. *Int. J. Climatol.* **25**, 693–712 (2005).

13. Asefi-Najafabady, S. & Saatchi, S. Response of African humid tropical forests to recent rainfall anomalies. *Philosophical Transactions of the Royal Society B-Biological Sciences* **368**, 20120306–20120306 (2013).

14. Malhi, Y. & Wright, J. Spatial patterns and recent trends in the climate of tropical rainforest regions. *Philosophical Transactions of the Royal Society B-Biological Sciences* **359**, 311–329 (2004).

15. van Engelen, V., Batjes, N., Dijkshoorn, K. & Huting, J. Harmonized world soil resources database (version 1.2). *FAO, IIASA, ISRIC, ISSCAS, JRC* (2012).

16. Hirota, M., Holmgren, M., Van Nes, E. H. & Scheffer, M. Global resilience of tropical forest and savanna to critical transitions. *Science* **334**, 232–235 (2011).

17. Potapov, P. *et al.* Mapping the world's intact forest landscapes by remote sensing. *Ecol. Soc.* **13** (2008).

18. Bartholomé, E. & Belward, A. S. GLC2000: A New Approach to Global Land Cover Mapping from Earth Observation Data. *Int. J. Remote Sens.* **26**, 1959–1977 (2005).

19. Staver, a. C., Archibald, S. & Levin, S. a. The global extent and determinants of savanna and forest as alternative biome states. *Science* **334**, 230–2 (2011).

20. Dakos, V. *et al.* Methods for detecting early warnings of critical transitions in time series illustrated using simulated ecological data. *PLOS ONE* **7** (2012).

21. Tsay, R. S. & Tiao, G. C. Consistent estimates of autoregressive parameters and extended sample autocorrelation function for stationary and nonstationary ARMA models. *Journal of the American Statistical Association* **79**, 84–96 (1984).

22. Fuller, W. A. *Introduction to Statistical Time Series* (John Wiley & Sons, New York, 1996), 2nd edn.

23. Verbesselt, J., Hyndman, R., Newnham, G. & Culvenor, D. Detecting trend and seasonal changes in satellite image time series. *Remote Sens. Environ.* **114**, 106–115 (2010).

24. Verbesselt, J., Zeileis, A. & Herold, M. Near real-time disturbance detection using satellite image time series. *Remote Sensing of Environment* **123**, 98–108 (2012).

25. Holt, C. C. Forecasting seasonals and trends by exponentially weighted moving averages. *International Journal of Forecasting* **20**, 5–10 (2004). URL http://ideas.repec.org/a/eee/intfor/v20y2004i1p5-10.html.

26. Winters, P. R. Forecasting sales by exponentially weighted moving averages. *Management Science* **6**, 324–342 (1960). URL http://pubsonline.informs.org/doi/abs/10.1287/mnsc.6.3.324. http://pubsonline.informs.org/doi/pdf/10.1287/mnsc.6.3.324.

27. Durbin, J. & SJ, K. *Time Series Analysis by State Space Methods* (Oxford University Press, 2001).

28. Hastie, T. & Tibshirani, R. *Generalized Additive Models* (Chapman & Hall/CRC, 1990).

29. Hastie, T. & Tibshirani, R. Varying-coefficient models. *Journal of the Royal Statistical Society B* **55**, 757–796 (1993).

30. Rosales, L. F. & Krivobokova, T. Instant Trend-Seasonal Decomposition of Time Series with Splines. Courant Research Centre: Poverty, Equity and Growth - Discussion Papers 131, Courant Research Centre PEG (2012). URL http://ideas.repec.org/p/got/gotcrc/131.html.

31. Cleveland, R. B., Cleveland, W. S., McRae, J. E. & Terpenning, I. STL: A seasonal-trend decomposition procedure based on loess. *Journal of Official Statistics* **6**, 3–73 (1990).

32. Kwiatkowski, D., Phillips, P., Schmidt, P. & Shin, Y. Testing the null hypothesis of stationarity against the alternative of a unit root. *Journal of Econometrics* **54**, 159–178 (1992).

33. Corbyn, J. Time series analysis with applications in R, 2nd edition. *Journal of the Royal Statistical Society Series a-Statistics in Society* **174**, 507–507 (2011).

34. Wood, S. N. *Generalized Additive Models: An Introduction with R* (Chapman & Hall/CRC, 2006).

DOI: 10.1038/NCLIMATE3108

35. Fahrmeir, L., Kneib, T., Lang, S. & Marx, B. *Regression – Models, Methods and Applications* (Springer-Verlag, Berlin, 2013). ISBN 978-3-642-34332-2.

36. R Development Core Team. *R: A Language and Environment for Statistical Computing*. R Foundation for Statistical Computing, Vienna, Austria (2013).

37. Hijmans, R. J. & van Etten, J. ***raster**: Geographic Data Analysis and Modeling* (2013). R package version 2.0-41.

38. Dethlefsen, C. & Lundbye-Christensen, S. Formulating state space models in R with focus on longitudinal regression models. *Journal of Statistical Software* **16**, 1–15 (2006). URL http://www.jstatsoft.org/v16/i01.

39. Dethlefsen, C., Lundbye-Christensen, S. & Christensen, A. L. ***sspir**: State Space Models in R* (2012). URL http://CRAN.R-project.org/package=sspir. R package version 0.2.10.

40. Wood, S. N. ***mgcv**: GAMs with GCV/AIC/REML Smoothness Estimation and GAMMs by PQL* (2013). R package version 1.7-22.